On the Tide-Induced Property Flux: Can It Be Locally Countergradient?*

HSIEN-WANG OU, CHANG-MING DONG, AND DAKE CHEN

Lamont-Doherty Earth Observatory, Columbia University, Palisades, New York

1 July 1998 and 29 September 1999

ABSTRACT

The horizontal property flux induced by tides is examined by both analytical and numerical models. It is found that this flux is highly heterogeneous in the vertical and may be directed up the mean gradient near the bottom. This countergradient tidal flux is a consequence of differing boundary conditions satisfied by velocity and property fields, and hence a robust feature. The corresponding tidal diffusivity is substantial where tides are strong and hence potentially important in the mean property balance.

1. Introduction

Tidal fronts are ubiquitous in coastal oceans. Prominent examples include that over the Georges Bank off the northeastern United States, which may extend to the outer shelf because of strong tides. How properties might be transported across a frontal boundary is a subject of longstanding interest because of its implications on biological productivity and dispersal of pollutants, among others. Studies on the cross-frontal exchange often focus on advection by the mean motion (e.g., Loder and Wright 1985), with less attention paid to tide-induced fluxes. These fluxes play a key role in studies of shear dispersion by oscillatory flows (e.g., Okubo 1967; Smith 1982), which however generally consider vertically averaged fields. We undertake to examine the vertical structure of tidal-induced property fluxes and show that they are highly heterogeneous, and may in fact be countergradient locally.

For the organization of the paper, we consider in section 2 a simple analytical model to elucidate the basic physics of tide-induced property flux. Solution from a primitive-equation numerical model is presented in section 3 to corroborate analytical results. The importance of this tide-induced flux is assessed in section 4.

2. Analytical model

For simplicity, let us consider a cross-shore plane on which a mean property field has vertical isolines (Fig.

1), and which is subject to a cross-shore tidal current. A Cartesian coordinate system is used with x and z axes pointing shoreward and upward respectively. For convenience of discussion, we use temperature as a proxy for the property field, which increases shoreward. With ''prime'' and ''overbar'' denoting tidal and mean variables respectively, let us consider tidal fields governed by the equations:

$$u'_t = -\rho_0^{-1} p'_x + \kappa^* u'_{zz}, \qquad (2.1)$$

$$T'_t + u'\overline{T}_x = \kappa^* T'_{zz}, \qquad (2.2)$$

where subscripts indicate partial derivatives, and κ^*, a vertical diffusivity, is assumed constant and applied to both momentum and property fields. For simplicity, we have neglected earth's rotation, which does not affect the basic mechanism. The earth's rotation is included in the numerical solution to be shown later. We have also neglected stratification so that the pressure gradient is vertically uniform and constitutes the external forcing for the tidal current. This tidal current interacts with the mean thermal gradient, which causes in turn temperature fluctuations. To isolate the tidal effect, we impose the boundary conditions that

$$u' = 0 \quad \text{at } z = 0, \qquad (2.3)$$

$$u'_z = 0 \quad \text{at } z = H, \quad \text{and} \qquad (2.4)$$

$$T'_z = 0 \quad \text{at } z = 0, h. \qquad (2.5)$$

That is, the surface is free of both stress and heat flux, and the bottom is nonslip and insulating. Given the local tidal forcing p'_x and mean thermal gradient $\overline{T}_x$, (2.1) through (2.5) can be solved at any x for the tidal fields u' and T', which can then be used to calculate the tidal flux $\overline{u'T'}$.

Before we proceed with the solution, it is trivial to see that, when vertically integrated, this tidal flux is

---

Corresponding author address: Hsien-Wang Ou, Lamont-Doherty Earth Observatory, Columbia University, Route 9W, Palisades, NY 10964.
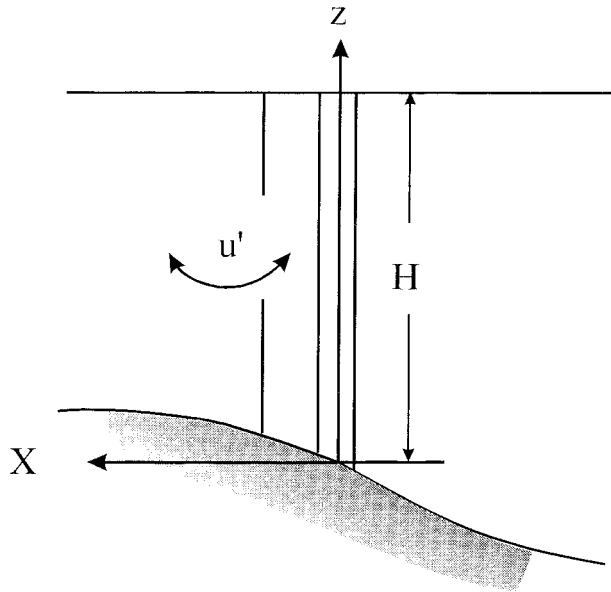E-mail: dou@ldeo.columbia.edu

FIG. 1. The model configuration for the analytical model, in which a cross-shore tidal current interacts with a mean property field having vertical isolines.
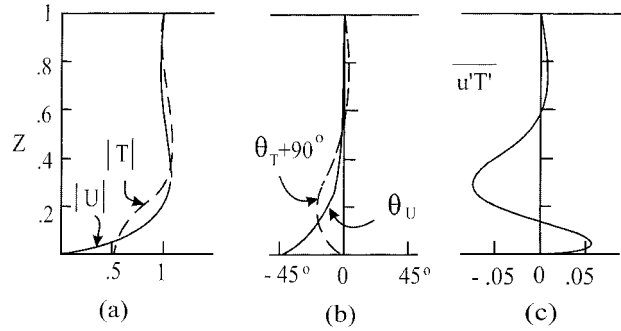

FIG. 2. Analytical solution for the case of $\kappa = 0.01$: (a) amplitude, (b) phase, and (c) the tidally induced horizontal flux.

downgradient, as one would expect from the second law of thermodynamics. Multiplying (2.2) with T', and averaging it over a tidal cycle, one obtains

$$\overline{u'T'}\,\overline{T}_x = \kappa^*\overline{T'T'_{zz}}, \tag{2.6}$$

which can be integrated vertically to yield [using the boundary conditions (2.5)]

$$\overline{T}_x \int_0^H \overline{u'T'}\, dz = -\kappa^* \int_0^H \overline{(T'_z)^2}\, dz < 0. \tag{2.7}$$

The two terms on the lhs are thus opposite in sign, or the vertical-averaged flux is directed down the mean gradient. We shall see later however, this tidal flux is highly heterogeneous in the vertical, and may reverse sign locally.

For convenience of the derivation, the variables are henceforth nondimensionalized according to following rules: z by the local water depth H, t' by σ^{-1} (σ being the tidal frequency), u' by $[u'] \equiv \sigma^{-1}\rho_0^{-1}|p'_x|$ (the absolute sign indicates the amplitude), and T' by $[T'] \equiv \sigma^{-1}[u']\overline{T}_x$. Defining the dimensionless diffusivity

$$\kappa = \kappa^*(\sigma H^2)^{-1}, \tag{2.8}$$

and expressing the tidal fields as complex variables of the form

$$u' = U(z)e^{-it}, \tag{2.9}$$

$$T' = T(z)e^{-it}, \tag{2.10}$$

the governing equations become

$$-iU = -i + \kappa U_{zz}, \tag{2.11}$$

$$-iT + U = \kappa T_{zz}, \tag{2.12}$$

with boundary conditions

$$U = 0 \quad \text{at } z = 0, \tag{2.13}$$

$$U_z = 0 \quad \text{at } z = 1, \quad \text{and} \tag{2.14}$$

$$T_z = 0 \quad \text{at } z = 0, 1. \tag{2.15}$$

For convenience, we have set the phase of the tidal forcing to be such that U is real in the absence of friction. The solution for U can be derived from (2.11), (2.13), and (2.14), which can be substituted into (2.12) to obtain a solution for T subject to the boundary conditions (2.15). The analytical solution of U and T is given in the appendix. Once the tidal fields are obtained, the tidal flux of heat can be calculated through the expression

$$\overline{u'T'} = \frac{1}{2}\,\text{Re}\{UT^*\}. \tag{2.16}$$

It is seen that the only dimensionless parameter that enters the governing equations (2.11) through (2.15) is the dimensionless diffusivity κ, which measures the importance of vertical mixing. We have plotted in Fig. 2 the solution for the case of $\kappa = 0.01$. The e-folding scale of the general solution (see appendix) is $(2\kappa)^{1/2} = 0.14$, which characterizes the height of the bottom boundary layer. As expected, the amplitude of tidal current is approximately unity in the interior, and decreases to zero at the bottom through the frictional boundary layer (Fig. 2a). It is interesting to note that the tidal current exhibits an upward phase propagation in the frictional boundary layer (Fig. 2b), consistent with previous studies (see, e.g., Fig. 4 of Loder and Wright 1985). This can be understood by noting that the general solution to (2.11) has a nonhomogeneous boundary condition at the bottom (see appendix), the signal of which thus propagates upward. Physically, in the bottom boundary layer, the tidal forcing is partially balanced by the stress acting on the instantaneous velocity, while in the interior the tidal forcing merely accelerates the flow which thus lags behind the flow near the bottom.

The total phase range should be within a quadrant or a few tens of degrees, as indicated in the figure.

Since the temperature signal is caused by the tidal current advecting the mean thermal gradient (2.12), its amplitude would mimic that of the tidal current were there no vertical mixing, which accounts for its general trend of an upward increase (Fig. 2a). But because the temperature fluctuation satisfies the zero-gradient rather than zero-amplitude condition at the bottom, its amplitude diminishes less severely than that of the tidal current in the bottom boundary layer. Nonetheless, this nonuniformity in the amplitude would cause a diffusive heat flux in the bottom boundary layer, which is downward (upward) during the warm (cool) cycle. Considering that the bottom is insulating, this heat flux would cause a downward phase propagation in the bottom boundary layer, opposite to that of the tidal current (Fig. 2b).

Since the two phase curves cross each other where the temperature gradient has a maximum [i.e., where the rhs of (2.12) vanishes so that the two fields are in quadrature], the horizontal heat flux thus is positive (countergradient) below this point and negative (downgradient) above, as indicated in Fig. 2c. Outside the influence of the bottom mixing, the phase curve of temperature must reverse slope so as to merge with that of the tidal current in the interior. There however could be a slight overshoot near the surface, resulting in a small positive heat flux. We have also calculated the solution (not shown) when κ is sufficiently large (say, of unity) that the whole water column is diffusive. As expected, the amplitude variation in both tidal current and temperature is lessened, and this is more so for the temperature field for the reason given above. Also the phase propagation for both fields becomes less distinct, resulting in a much-reduced tidal flux.

The analytical solution has thus shown that horizontal heat flux induced by tides is highly nonuniform in the vertical and can have both signs. Near the bottom, in particular, this heat flux is directed up the mean gradient. To explain this physically, let us imagine we are at the peak of the ebb cycle, so that the tidal current is directed offshore, which causes the local temperature to rise, reaching a maximum a quarter cycle later. Since the magnitude of the temperature change mimics somewhat that of the tidal current, there would be a downward diffusion of heat, causing the temperature to rise above the insulating bottom. This warming reaches a maximum another quarter cycle later, by which time the tidal current has reversed, or a warm anomaly is correlated with an onshore current. Similarly in the next half of the tidal cycle, a cold anomaly is correlated with an offshore current, so that the net flux averaged over a tidal cycle is countergradient. Farther up the water column, above the point of maximum temperature gradient, the same argument leads to a tidal flux of the opposite sign.

For a further examination of the tidal flux, its vertical
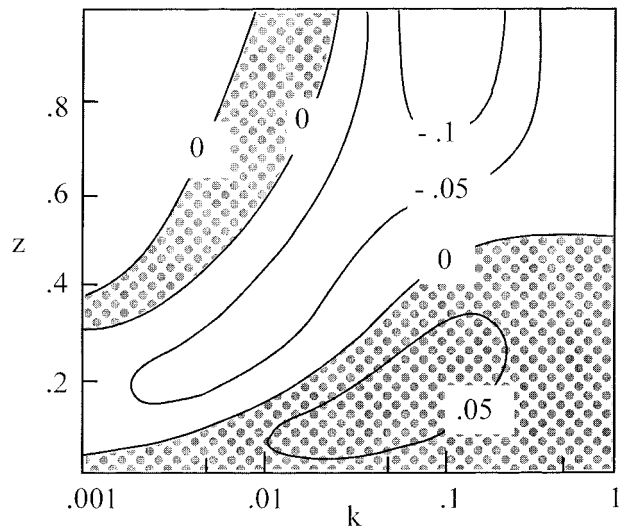

FIG. 3. Tidal heat flux as a function of the dimensionless diffusivity κ and height above bottom, calculated from the analytical solution.

distribution is calculated and plotted in Fig. 3 as a function of the tidal diffusivity κ. In the inviscid limit, the heat flux vanishes since temperature and current fluctuations are in quadrature (as the bottom boundary layer is infinitely thin). As κ increases, the nonzero heat flux begins to emerge in the bottom boundary layer, which grows to occupy the whole water column when κ reaches $O(0.1)$, and heat flux attains a maximum of $O(0.1)$. As κ increases further, the heat flux begins to diminish and approaches zero as vertical mixing erases the vertical phase propagation. We have so far considered an analytical model to elucidate the basic mechanism for the countergradient tidal flux. We shall next present the solution from a primitive-equation numerical model, and show that it corroborates the analytical results.

3. Numerical solution

The numerical model used is a primitive-equation model based on second-moment turbulence closure and which solves interactive thermal and dynamical fields (Chen and Wang 1990). For the present purpose, the model is configured on a two-dimensional cross-shore plane as shown schematically in Fig. 4, with horizontal and vertical grid spacing of 2 km and 3 m, respectively. The boundary conditions at the top and bottom surfaces are the same as that of the analytical model except a stress condition (instead of nonslip) is applied at the bottom. At the inshore boundary, velocity has zero normal-gradient, and temperature is set at a fixed value of 12°C, which provides a buoyancy source for the generation of the thermal front. At the offshore boundary, zero normal-gradient condition is imposed for both velocity and temperature. At $t = 0$, the whole fluid except that near the inshore boundary is set at 6°C, which merges linearly to the boundary value of 12°C over six grids,
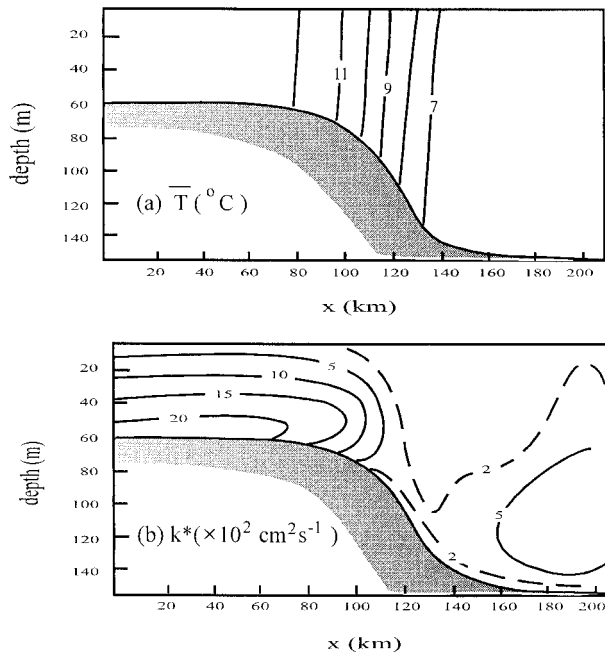
FIG. 4. Contours of (a) mean temperature and (b) vertical diffusivity, calculated from the numerical model.
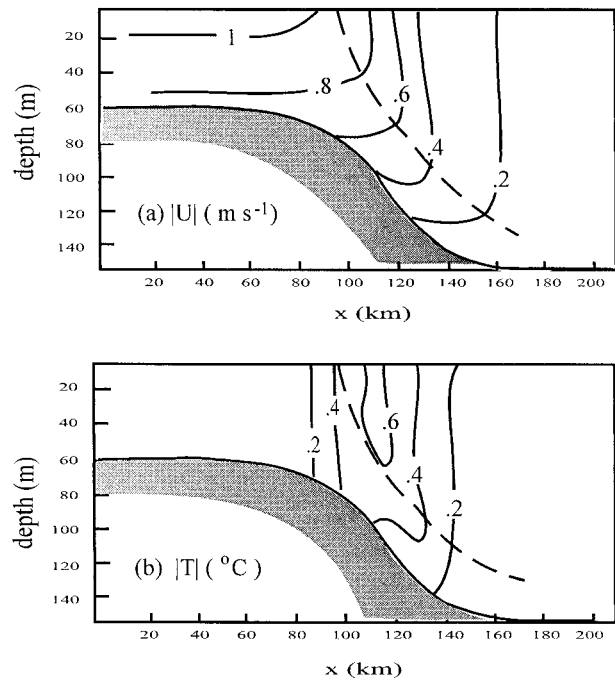
FIG. 5. Same as Fig. 4, but for the amplitude of (a) the tidal current and (b) temperature.

and tidal current is switched on by imposing a periodical surface at the offshore end that is of semidiurnal frequency. The amplitude of the forcing is adjusted so that the maximum tidal current (i.e., at the shallow end) is about 1 m s^{-1}. The topography and the tidal amplitude used are intended to be representative of that over Georges Bank. The strong tidal mixing over the shallow shelf causes the initially sharp temperature gradient at the inshore boundary to smooth out and move offshore until it reaches the shelf break when a quasi-steady state is established (after about 300 days).

The mean thermal field of this state is plotted in Fig. 4a, which exhibits a frontal structure, accompanied by an along-shore mean flow (not shown) that reaches 30 cm s^{-1} at the surface. The vertical diffusivity is plotted in Fig. 4b, which decreases rapidly offshore near the shelf break as the tidal current weakens. It shows a secondary maximum offshore because of vanishing stratification (hence reduced Richardson number).

The amplitude of tidal current is plotted in Fig. 5a. As expected, the tidal current intensifies shoreward as bottom shoals because of continuity. Its amplitude is vertically uniform in the interior but diminishes downward within the friction boundary layer, the top of which thus as marked by the dashed curve. For the particular case considered here, it is seen that the whole shelf is frictional. The amplitude of the temperature field is plotted in Fig. 5b. Since the temperature signal is generated by tidal current advecting the mean thermal gradient, it is largely confined to the frontal zone. Its amplitude is vertically uniform in the interior, just as the tidal current,

but its reduction in the boundary layer is considerably less distinct, as explained earlier.

The phase of the tidal current is shown in Fig. 6a. Consistent with the analytical solution, the signal propagates upward, which is particularly prominent where
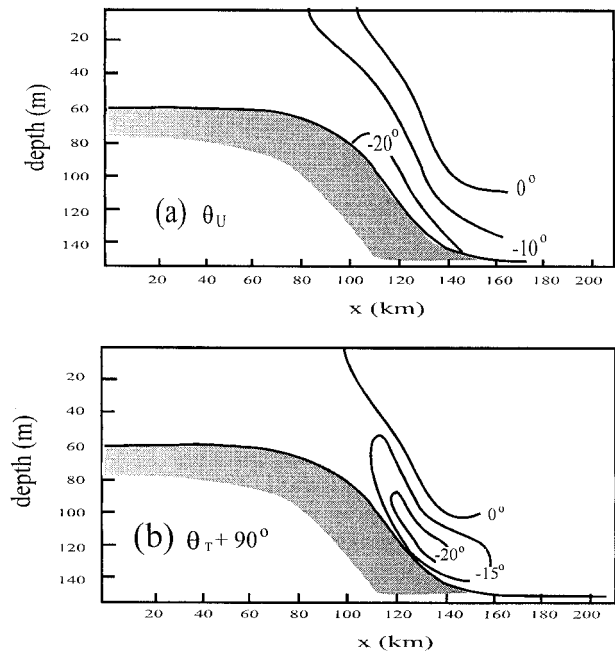
FIG. 6. Same as Fig. 4, but for the phase of (a) the tidal current and (b) temperature.
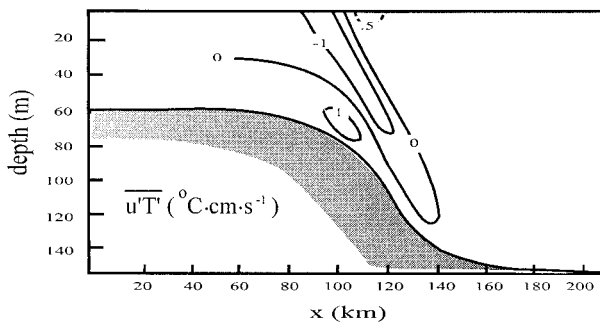
FIG. 7. Same as Fig. 4, but for the tide-induced horizontal heat flux.

there is a distinct frictional boundary layer. Over the shelf, large vertical mixing has erased the phase propagation. The phase for the temperature field, which has been displaced by 90°, is shown in Fig. 6b. It has a similar pattern as that of the tidal current except near the bottom where the direction of phase propagation is reversed, just as predicted by the analytical solution (Fig. 2).

Because of this difference in phase distribution, the heat flux, as plotted in Fig. 7, shows a positive value (countergradient) near the bottom and negative above, consistent with the analytical solution. Since κ used in Fig. 3 increases with enhanced vertical diffusivity and shoaling bottom (2.8), the progression of κ in Fig. 3 can be compared with the shoreward progression in Fig. 7. The qualitative agreement of the two is readily seen, including the presence of a small positive heat flux near the surface.

For quantitative comparison of the two, however, one is mindful of the differences of the two models, including a constant diffusivity and nonslip condition used in the analytical model. Despite these differences, one still expects the two heat fluxes to be of the same order of magnitude. As an example, let us select the location 120 km offshore in the numerical model where the depth is about 100 m, and an average diffusivity κ^* is about 100 cm^2 s^{-1}, which yields $\kappa = 7 \times 10^{-3}$ [from (2.8)]. Based on Fig. 3, one estimates a maximum countergradient heat flux of about 0.03. To translate this into dimensional value, we estimate from Fig. 5 amplitudes for tidal current and temperature (at the surface, which define the scales) to be 50 cm s^{-1} and 0.5°C, respectively, so that the above heat flux corresponds to a dimensional value of 0.75°C cm s^{-1}. When compared with Fig. 7, this value is of the same order. These comparisons suggest that the analytical model has captured the essential features exhibited in the numerical model, the latter of which thus can be explained by the physical mechanism discussed earlier.

4. Discussion

The obvious question is the significance of this tidally induced flux. One way to assess its importance is to calculate the effective tidal diffusivity κ_T^* defined by the expression

$$\overline{u'T'} = -\kappa_T^* \overline{T}_x. \qquad (4.1)$$

As an example, let us choose the same upper-slope location as above (i.e., 120 km offshore) where the on-shore heat flux has a magnitude of about 0.5°C cm s^{-1} and the mean temperature gradient is about 0.1°C km^{-1}. Substituting these values into (4.1), one obtains a tidal diffusivity κ_T^* of about -5×10^5 cm^2 s^{-1}. Its magnitude is greater than values typically used in coastal models (the value used in our numerical model is 2×10^5 cm^2 s^{-1}. But more importantly, it is negative.

Another way to assess its importance is to compare its effect with that of mean advection. Let L and $\overline{U}$ denote characteristic scales of the frontal width and mean cross-frontal velocity, respectively, then the timescales associated with tidal diffusion and mean advection are given by $(\kappa_T^*)^{-1}L^2$ and $\overline{U}^{-1}L$, respectively. The relative importance of the two can be measured by their ratio, or the Peclet number $(\kappa_T^*)^{-1}\overline{U}L$. Using the above value of tidal diffusivity and a frontal scale L of $O(10$ km), the Peclet number is of $O(1)$ or smaller if $\overline{U} \leq O(0.5$ cm s$^{-1})$. Since the latter typically characterizes the magnitude of the mean cross-frontal velocity (e.g., Houghton 1997), the mechanism discussed here could be comparable to the mean advection for the tidal regime considered here.

This tidal diffusivity obviously depends strongly on the tidal amplitude. To assess this dependence from the analytical solution, one derives from (4.1) and the scales used to nondimensionalize heat flux that

$$\kappa_T^* = -\overline{u'T'}\sigma^{-1}[u']^2, \qquad (4.2)$$

where $\overline{u'T'}$ is the nondimensionalized heat flux shown in Fig. 3. One notes first of all that although a nonzero tidal heat flux requires the presence of a mean thermal gradient—the reason that it is largely confined to the frontal zone in Fig. 7—the tidal diffusivity is independent of the mean thermal field since the latter does not enter the nondimensionalized heat flux. In other words, tidal diffusivity is a function of the tidal amplitude, independent of the mean field.

Second, the tidal amplitude affects the tidal diffusivity through both its explicit appearance in (4.2) and its effect on $\overline{u'T'}$ (through κ^* and hence κ). Based on Fig. 3 however, this latter effect is small over a wide range of tidal amplitude: the maximum $\overline{u'T'}$ is of $O(0.05)$ ranging from the weak-tide case when the frictional boundary layer spans a small portion of the water column, up to the case when the frictional boundary layer begins to fill up the whole water column. Within this wide range, the tidal diffusivity thus is roughly quadratic in the tidal amplitude. The value estimated above over the upper slope therefore can be considerably greater farther inshore where tidal current is stronger, possibly augmenting its importance.

We have used temperature merely as a proxy for pas-

sive properties that are conserved. The transport of such property across frontal boundary has received renewed interest on account of newly acquired data. Monitoring dye concentration at the foot of a shelf-break front, Houghton (1997) found that the front poses a significant barrier for its transport in the bottom boundary layer, consistent with model simulation of Chapman and Lentz (1994), which contains no tides. Could the countergradient flux discussed here provide an additional mechanism that inhibits tracer dispersion in the bottom boundary layer? When attempting observational validation of this countergradient heat flux, one is mindful of many other contributors to the observed flux, and the fact that this flux stems from vertical mixing which invariably acts to lessen its differential effect on the mean fields.

APPENDIX

Tidal Solution

The solution to (2.9) is

$$U = 1 + a_1 e^{r_1 z} + a_2 e^{r_2 z}, \tag{A.1}$$

where

$$r_1 = (2\kappa)^{-1/2}(1 - i), \tag{A.2}$$

$$r_2 = -(2\kappa)^{-1/2}(1 - i), \tag{A.3}$$

and the two integration constants a_1 and a_2 are determined by the boundary conditions (2.11) and (2.12) to be

$$a_1 = (r_1 e^{r_1} - r_2 e^{r_2})^{-1} r_2 e^{r_2}, \tag{A.4}$$

$$a_2 = -(r_1 e^{r_1} - r_2 e^{r_2})^{-1} r_1 e^{r_1}. \tag{A.5}$$

Substituting (A.1) into (2.1), and using the boundary condition (2.13), one derives the solution for T of the form

$$T = T_p + b_1 e^{r_1 z} + b_2 e^{r_2 z}, \tag{A.6}$$

where T_P is the particular solution given by

$$T_P = -i + \frac{z}{\kappa(r_1 - r_2)}(a_1 e^{r_1 z} - a_2 e^{r_2 z}), \quad \text{and} \tag{A.7}$$

$$b_1 = \frac{1}{\kappa r_1 (r_1 - r_2)(e^{r_1} - e^{r_2})}$$
$$\times \{a_1[e^{r_2} - (r_1 + 1)e^{r_1}] + a_2 r_2 e^{r_2}\}, \tag{A.8}$$

$$b_2 = \frac{1}{\kappa r_2 (r_1 - r_2)(e^{r_1} - e^{r_2})}$$
$$\times \{a_1 r_1 e^{r_1} + a_2[e^{r_1} - (r_2 + 1)e^{r_2}]\}, \tag{A.9}$$

REFERENCES

Chapman, D. C., and S. J. Lentz, 1994: Trapping of a coastal density front by the bottom boundary layer. *J. Phys. Oceanogr.,* **24,** 1464–1479.

Chen, D., and D.-P. Wang, 1990: Simulating the time-variable coastal upwelling during CODE 2. *J. Mar. Res.,* **48,** 335–358.

Houghton, R. W., 1997: Lagrangian flow at the foot of a shelfbreak front using a dye tracer injected into the bottom boundary layer. *Geophys. Res. Lett.,* **24,** 2035–2038.

Loder, J. W., and D. G. Wright, 1985: Tidal rectification and frontal circulation on the sides of Georges Bank. *J. Mar. Res.,* **43,** 581–604.

Okubo, A., 1967: The effect of shear in an oscillatory current on horizontal diffusion from an instantaneous source. *Int. J. Oceanol. Limnol.,* **1,** 194–204.

Smith, R., 1982: Contaminant dispersion in oscillatory flows. *J. Fluid Mech.,* **114,** 379–398.